J Solid State Electrochem (1999) 3: 337–347

ORIGINAL PAPER

Juan Bisquert · Germà Garcia-Belmonte
Francisco Fabregat-Santiago

Modelling the electric potential distribution in the dark in nanoporous semiconductor electrodes

Received: 25 June 1998 / Accepted: 15 December 1998

Abstract This study concerns the electric potential distribution in the dark in nanocrystalline porous semiconductor electrodes, in full depletion conditions. Since band bending in a single colloidal particle is small, the idea is to develop a model that accounts for the total potential drop resulting from the equilibration between the Fermi level and the redox potential in the solution. As preliminary steps, the band bending and potential distribution in a planar electrode and also in a colloidal semiconductor particle are reviewed. In order to overcome the limitations of results based on these geometries, a model based on a columnar shape is developed. The Poisson equation is solved in the columnar electrode, with careful consideration of the boundary conditions. A large potential drop is shown to take place at the back contact. To complete the study, the effect of the depletion zone in the transparent conducting oxide is analysed. Simple expressions are derived that permit evaluation of how the total potential drop is distributed between the electrode and the substrate. From this, the strength and spatial range of the electric field in the electrode can be estimated.

Key words Photoelectrochemistry · Porous nanocrystalline electrodes · Potential distribution Titanium dioxide films

Introduction

The photoelectrochemical response of a planar semiconductor electrode is governed by the electric fields at the surface. The depletion zone already formed in dark conditions is largely responsible for efficient charge separation. In quantitative terms, the dependence of quantum efficiency on the applied voltage and wavelength is usually described by Butler's application [1] of the Gärtner model [2] for illuminated Schottky barriers.

In recent years, a new class of photoelectrochemical device based on porous nanocrystalline semiconductor films has raised much attention [3]. Nanostructured electrodes are composed of small, lightly doped particles of diameter ranging from 5 to 50 nm, that are partly sintered together to form a porous film. The porous structure is interpenetrated by the electrolyte all the way up to the back contact. High quantum efficiencies have been observed many times in dye-sensitized sintered colloidal TiO_2 films. It is expected from the outset that the geometry exerts a considerable influence on the device operation.

It was natural to inquire if the presence of an electric field could explain the observed photocurrents by means of the Gärtner mechanism. In this respect, a calculation by Albery and Bartlett for colloidal semiconductor particles [4] was adapted to nanoporous TiO_2 electrodes by Grätzel and co-workers [5, 6], who suggested that owing to the very small particle size in combination with the low doping density, no significant potential drop should be present between the centre and the surface of an individual semiconductor particle. This was an influential proposal indeed, in that thereafter it has generally been assumed that the role of electric fields in nanoporous electrodes should be discarded [7–11], or equivalently, that the Fermi level in the TiO_2 film is essentially flat.

An early finding on nanoporous electrodes was that when illuminating the cell from the substrate side, larger photoinduced currents resulted than when repeating the experiment illuminating from the electrolyte side [7, 12, 13]. This is the opposite situation to that found in, for example, a flat polycrystalline TiO_2 electrode [14], where illumination through the electrolyte produces the larger response. These findings appeared consistent with an absence of large electric fields in nanoporous TiO_2 electrodes, and models have been proposed [7, 10, 15] in which the transport of photogenerated electrons is driven by diffusion only. Nonetheless, some workers have found experimental evidence pointing to the

J. Bisquert (✉) · G. Garcia-Belmonte · F. Fabregat-Santiago
Departament de Ciències Experimentals,
Universitat Jaume I, E-12080 Castelló, Spain
e-mail: bisquert@uji.es

existence of electric fields near the back contact under certain conditions. This occurred with electroreflectance measurements [9], with electrochemical impedance spectroscopy measurements [16] and with time-resolved photocharge measurements [17].

Without losing from sight the growing multiplicity of experimental results, here we wish to bring to focus a key idea in studies of the semiconductor/electrolyte junction, as the following: equilibration between the Fermi level and the redox potential forces a potential drop to be accommodated *in the semiconductor*. As formerly indicated, this is the notion that provides the basic element in the Gärtner-Butler model. In the case of a nanoporous electrode, however, a convincing explanation seems not to have been provided about the exact location of the potential drop. That the band bending at a certain part of the system is small is not a sufficient argument whereby most of the total potential drop must be disregarded. Several authors have in fact expressed their suspicions in this sense, for example Grätzel and coworkers [5] indicate that "The clustering and interconnection of the particles is expected to affect the potential distribution, and more significant electric fields are likely to be developed in such an array as compared to individual colloidal particles", and Bosschloo et al. [9] claim that "The nanoporous TiO_2 film is ... regarded as a dielectric rather than a semiconductor surface layer, and can, therefore, sustain a macroscopic electric field...".

In this context, the aim of the present work is to achieve a coherent picture of potential distribution which allows simple and quantitative statements to be made. Our strategy is to translate established ideas about a semiconductor/electrolyte junction in equilibrium to the peculiar porous geometry, and explore the possibilities. Hence we avoid entering into complexities such as interface charge states, though recognizing that this may be found to be necessary in further developments.

We begin with a brief revision of the properties of the distribution of electric charge and potential in a planar semiconductor in contact with a solution. This serves to fix the concepts used in the rest of the work. A critical appraisal is conducted on the application of the Albery-Bartlett model to TiO_2 nanoporous electrodes. Since we are led to conclude that a proper description of the potential distribution cannot be obtained on the basis of the single sphere model, we consider an alternative geometry based on a columnar shape to model the nanoporous structure, and the location of the missing potential drop is revealed. In addition, the dependence of the resulting electric field on the properties of the contact between the electrode and the substrate is studied.

Potential distribution and free electron density in flat geometry

We recall some basic facts (see e.g. [18]) regarding band bending in a planar (non-porous) n-type semiconductor electrode, schematized in Fig. 1. The curvature of the bands is described by Poisson's equation:

$$\nabla^2 V = -\frac{\rho}{\epsilon} \tag{1}$$

where V is the electric potential and ϵ is the dielectric constant of the semiconductor. For the cases of interest here (large gap semiconductor), it can be assumed that the minority carrier concentration is everywhere negligible (this implies that the surface band bending is not large enough to form an inversion layer), and hence the charge density is

$$\rho = q[N_D - n] \tag{2}$$

where N_D is the donor density, n is the density of free electrons, and q is the fundamental electric charge. For the following, it is convenient to introduce the reduced potential

$$\phi = -\frac{qV}{kT} \tag{3}$$

where k is the Boltzmann constant and T the temperature, so that $|\phi| = 1$ corresponds to the thermal voltage, 26 mV. Note the negative sign in Eq. 3 which makes the graphic representation of ϕ similar to that of the energy band edges. Scaling of energies to the thermal energy of 0.026 eV will also be used throughout this paper, e.g. we define a reduced Fermi level energy as

$$\varepsilon_F = E_F/kT \tag{4}$$

For a non-degenerate semiconductor we can use the Boltzmann statistics

$$n = N_c \exp[-(E_c - E_F)/kT] \tag{5}$$

where N_c is the effective density of states in the conduction band. A suitable reference for the electric

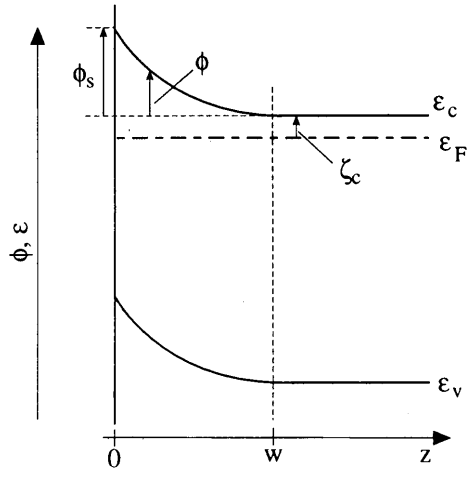

Fig. 1 Scheme of the energy band edges and reduced potential ϕ in a planar n-type semiconductor electrode, showing the notation used in this work. The junction with the electrolyte is at $z = 0$. ε_F is the Fermi level, ε_c is the lower edge of the conduction band, and ε_v is the upper edge of the valence band

potential $V = 0$ can be taken at the quasi-neutral region, so that the distance between the conduction band edge and the Fermi level is given at any point by

$$E_c - E_F = (E_{cb} - E_F) - qV \tag{6}$$

Here E_{cb} is the conduction band edge in the bulk, where the charge neutrality condition $n = n_b = N_D$ holds. In terms of the scaled magnitudes, Eq. 6 reads

$$\varepsilon_c - \varepsilon_F = \zeta_c + \phi \tag{7}$$

and obviously ζ_c is a material property:

$$\zeta_c = \varepsilon_{cb} - \varepsilon_F = \ln(N_c/n_b) \tag{8}$$

Hence Eq. 7 constitutes a suitable definition of potential ϕ even if there is no quasi-neutral region in the electrode, as turns out to happen in the cases discussed below. Note that the local free electron distribution can be written

$$n = N_D \exp(-\phi) \tag{9}$$

Introducing the extrinsic Debye length $L_D = (\epsilon kT/N_D q^2)^{1/2}$ and taking Eq. 9 into account, Eq. 1 can be written

$$\nabla^2\phi = \frac{1}{L_D^2}[1 - \exp(-\phi)] \tag{10}$$

Although, in the case of a planar geometry, Eq. 10 can be integrated exactly, several approximate forms of the right-hand side expression are often distinguished in certain regimes of potential ϕ in order to obtain simple, partially valid solutions. The weak band bending condition $|\phi| \ll 1$ leads to a linealized Poisson-Boltzmann equation:

$$\nabla^2\phi = \frac{1}{L_D^2}\phi \tag{11}$$

The full depletion condition $\phi \gg 1$ gives

$$\nabla^2\phi = \frac{1}{L_D^2} \tag{12}$$

and finally one has an accumulation layer when $\phi \ll -1$ with

$$\nabla^2\phi = -\frac{1}{L_D^2}\exp(-\phi) \tag{13}$$

Equations 11 and 13 have been written down mainly to stress the fact that the value of ϕ dictates the basic differential equation that has to be solved. Of primary interest here is the full depletion condition in Eq. 12, which according to the famous model by Schottky gives a space-charge region with parabolic bending near the junction:

$$\phi(z) = \frac{1}{2L_D^2}(z - w)^2 \tag{14}$$

and a free-field zone in the quasi-neutral region of the semiconductor (see Fig. 1). The surface potential ϕ_s indicated in Fig. 1 gives the total internal potential drop in the semiconductor:

$$\phi(0) = \phi_s \tag{15}$$

and from Eq. 14 the width of the depletion zone is given by

$$w = (2\phi_s)^{1/2} L_D \tag{16}$$

The internal drop ϕ_s may be varied by means of an externally applied potential, and according to Eq. 16 a displacement of the inner edge of the depletion zone results. It is worth noting that the total potential difference developed across the interface must include a potential drop across the Helmholtz layer and surface charges. It is apparent from Eq. 15 that ϕ_s is taken here as the potential at the outer edge of the depletion layer, and thus it does not include the drop at surface charge states.

The spherical particle

The Albery-Bartlett (A-B) model for colloidal semiconductors

Our general objective is to apply to nanoporous film electrodes the ideas concerning electric potential distribution which we have just reviewed. A convenient starting point is the useful A-B calculation [4]. These authors solved the Poisson equation for a spherical depleted semiconductor, employing a similar approach to that of Schottky for the planar electrode case. In the following paragraphs we outline the A-B model for a particle of radius a, distinguishing two situations: the partially depleted sphere and the fully depleted sphere. To facilitate discussion we formulate the model in terms of the potential ϕ defined in Eq. 7, which is linked to the local concentration of electrons by Eq. 9.

The sphere is not fully depleted

Full depletion is assumed to occur only in the layer $r_w \le r \le a$, (Fig. 2a), where the potential is distributed according to the Poisson equation (see Eq. 12):

$$\frac{1}{r^2}\frac{\partial}{\partial r}\left(r^2\frac{\partial\phi}{\partial r}\right) = \frac{1}{L_D^2} \tag{17}$$

In the inner spherical region of radius r_w, where quasi-neutrality conditions prevail, we must set $\phi = 0$ in the same fashion as in the planar electrode seen previously. Consequently at the inside edge of the depletion layer $r = r_w$ we have the boundary conditions $\partial\phi/\partial r = 0$ and $\phi(r_w) = 0$. Integration of Eq. 17 gives the result

$$\phi = \frac{1}{6L_D^2}\left[r^2 - 3r_w^2 + 2\frac{r_w^3}{r}\right] \quad (r_w \le r \le a) \tag{18}$$

which is sketched in Fig. 2a.

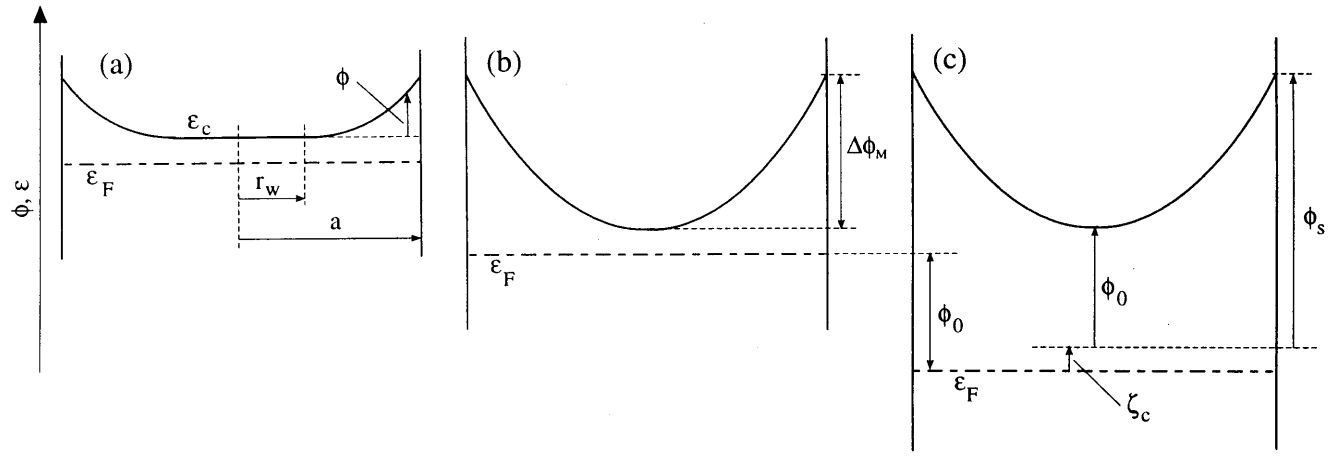

Fig. 2a–c Scheme of the energy band edges and reduced potential ϕ in a spherical n-type semiconductor particle of radius a. Three cases are shown: **a** partially depleted particle; **b** fully depleted particle with $\phi_0 = 0$; **c** fully depleted particle with $\phi_0 > 0$

Fully depleted sphere

Now $n \ll N_D$ in the whole spherical region, and again we must solve Eq. 17. We state the two boundary conditions at the central point: $\partial\phi/\partial r = 0$ and $\phi(r = 0) = \phi_0$, and we obtain

$$\phi = \phi_0 + \frac{1}{6}\left(\frac{r}{L_D}\right)^2 \tag{19}$$

The surface potential is given by

$$\phi_s = \phi_0 + \Delta\phi_M \tag{20}$$

where

$$\Delta\phi_M = \frac{1}{6}\left(\frac{a}{L_D}\right)^2 \tag{21}$$

is the maximum attainable potential drop between the centre and the surface of the semiconductor particle. An estimation of the extrinsic Debye length for colloidal TiO_2 particles in a nanoporous electrode with $N_D = 10^{17}$ cm^{-3} and $\epsilon = 130\epsilon_0$ gives $L_D \approx 40$ nm. If we take a typical particle size of say 20 nm, the total band bending as obtained from Eq. 21 is then smaller than the thermal energy.

The particular case $\phi_0 = 0$ corresponds to shrink to $r_w = 0$ the field-free region of the non-depleted sphere case (Eq. 18):

$$\phi = \frac{1}{6}\left(\frac{r}{L_D}\right)^2 \tag{22}$$

This is the curve sketched in Fig. 2b. However, in general $\phi_0 > 0$, and the Fermi level is shifted downwards with respect to the conduction band edge by an amount $kT\phi_0$ (assuming that the energy band edges are pinned [19]), (Fig. 2c). Note as a peculiar feature of the general solution, Eq. 19, that we do not have a zone, nor a point, where $\phi = 0$. The significance of ϕ_0 will be better appreciated with the following remark. Assume that $\phi_0 = 0$ so that Eq. 22 is the good solution. However, if $a < L_D$, which as we have just seen is a most frequent case, then we see from Eq. 22 that $\phi < 1$ everywhere in the sphere, which means that the Fermi level is too close to the conduction band edge to provoke full depletion. In this situation the A-B model cannot be consistently applied, and one should turn instead to Eq.11. The general solution (Eq. 19) is indeed valid as long as full depletion is warranted by the condition $\phi_0 \gg 1$.

The potential at the central point of the sphere

A remaining question is how the value of ϕ_0 is fixed in a given situation. For clarity, we treat separately the case of an isolated particle, and the case of a serial arrangement of connected particles in touch with a conducting substrate at one extreme.

In an isolated spherical particle the Fermi level must equilibrate the redox potential in the electrolyte. The necessary potential drop cannot be absorbed by the small band bending $\Delta\phi_M$ and consequently in equilibrium the ϕ-potential at the centre is not zero, but ϕ_0. Therefore we are concerned by the suggestion by others [6, 20] that if majority carriers deplete from a colloidal semiconductor which allows only a small degree of band bending, the electrical potential difference resulting from the transfer of charge from the semiconductor to the solution has to drop within the Helmholtz layer. In effect, as we have already pointed out, depletion necessarily requires that $\phi_0 \gg 1$. If the potential difference that is needed for equilibration of the Fermi level and redox potential goes entirely to the Helmholtz layer, then $\phi < 1$ in the sphere and depletion is negligible.

Let us turn to the situation of connected particles, which is intended to model the nanoporous TiO_2 electrode. Results of electrochemical impedance spectroscopy [8, 16] show that under a positive applied voltage the semiconductor array of particles is highly insulating. Hence we take for granted that substantial depletion occurs in practical situations, as we expect from basic principles.

Consider for definiteness a columnar array of spheres that stands on top of a tin oxide substrate (which in turn is in contact with the counter electrode) and normal to it. It is reasonable to expect that far from the substrate the A-B model approximately applies to each particle. This assumption has two consequences: that for all those particles the ϕ_0 value must be the same, and that this ϕ_0 value must correspond to the one attained if the particles were isolated in the electrolyte. On the other hand, and neglecting temporarily the potential drop in the substrate, for the particle that contacts the substrate we see that $\phi = 0$ at one side of it, while $\phi \approx \phi_0 \gg 1$ at the opposite side where it contacts another particle. Here the A-B model is not useful. Hence we may conjecture that for a nanoporous electrode composed of small, low-doped particles ($a < L_D$), the first few particles near the substrate take in most of the total potential drop ϕ_s, whereas each of the rest of particles shows only a small band curvature from the centre to the surface, as described by the A-B model.

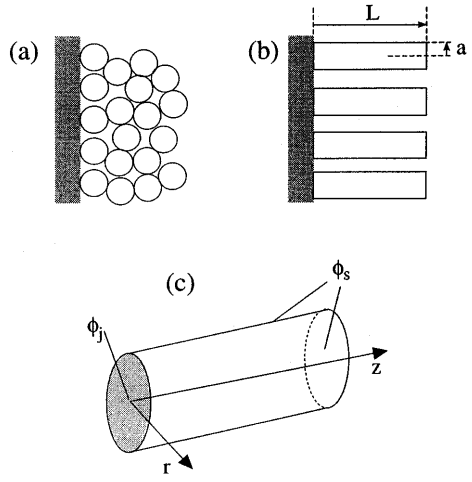

Fig. 3a–c Schematic representations of a nanoporous electrode. **a** An array of connected spherical particles. **b** A bundle of columnar particles. **c** View of a columnar particle showing the coordinate system; the *shaded circle* represents the junction with the substrate

The columnar model

Next we are interested in the development of a simple quantitative model of a connected array of particles that are depleted of free carriers. To this end we take a representative perfect column, or cylinder, which from an analytical point of view is more tractable than a chain of spheres. The radius of the column is a and its length (thickness of the electrode) is L, and it is assumed that $L \gg a$. The columnar geometry has already been used by other authors in relation to depleted porous electrodes [8, 21]. The complete electrode consists of a bundle of parallel columnar particles attached to a transparent conducting oxide (Fig. 3b). Each columnar particle is a dielectric with uniform charge density N_D. Naming r and z the radial and axial cylindrical coordinates as in Fig. 3c, from Eq. 12 we must solve

$$\frac{1}{r}\frac{\partial}{\partial r}\left(r\frac{\partial \phi}{\partial r}\right) + \frac{\partial^2 \phi}{\partial z^2} = \frac{1}{L_D^2} \tag{23}$$

We split the solution into two parts

$$\phi(r,z) = \phi^{\mathscr{L}}(r,z) + \phi^{\mathscr{P}}(r,z) \tag{24}$$

which satisfy in turn the Laplace equation

$$\nabla^2 \phi^{\mathscr{L}} = 0 \tag{25}$$

and the Poisson equation with homogeneous Dirichlet boundary conditions:

$$\nabla^2 \phi^{\mathscr{P}} = \frac{1}{L_D^2} \tag{26}$$

$$\phi^{\mathscr{P}}(r,L) = \phi^{\mathscr{P}}(a,z) = \phi^{\mathscr{P}}(r,0) = 0 \tag{27}$$

Any inhomogeneous boundary conditions that we decide to utilize in the full solution must be set on the Laplace part of the solution. We will use here the following.

Potential at the surfaces of the column

Surfaces in contact with the electrolyte

We set the surfaces surrounded by the electrolyte at a constant potential

$$\phi^{\mathscr{L}}(r,L) = \phi^{\mathscr{L}}(a,z) = \phi_s \tag{28}$$

This is a major assumption in the model, equivalent to the assumption that the potential drop at the Helmholtz layer and surface states is independent of the position along the surface. In a more advanced treatment, a distributed potential along the semiconductor surface should be considered, in principle.

Surface in contact with the substrate

Were the substrate a metal, we could simply set $\phi = 0$ at the shaded circle $z = 0$ in Fig. 3c. In the problem under consideration, however, it appears more appropriate to treat the contact as an abrupt heterojunction in which a part of the total potential drop ϕ_s may lie in a depletion zone at the transparent conducting oxide. Strict adhesion to the columnar geometry would lead us to solve a two-dimensional Poisson equation *in the substrate* together with Eqs. 25 and 28 and match both functions via the continuity condition of the electric displacement field across the two dielectrics (see below). However, this cumbersome procedure seems unnecessary in view of the fact that we ignore the detailed properties of the real

contact. Instead, we examine in the framework of the column model *two* suitable forms of the potential at the junction with the substrate. This permits comparison of their respective effects on the overall potential distribution in the electrode, and to choose later the path of greater simplicity.

A first example consists in setting the circle at the junction at a constant value:

$$\phi^{\mathscr{L}\mathrm{I}}(r,0) = \phi_\mathrm{j} \quad r < a \tag{29}$$

In our second choice the potential varies smoothly from the value ϕ_j at the centre of the circle, to ϕ_s at the edge:

$$\phi^{\mathscr{L}\mathrm{II}}(r,0) = \phi_\mathrm{s} + (\phi_\mathrm{j} - \phi_\mathrm{s})J_0(r/d) \tag{30}$$

Here J_0 is the Bessel function of order zero, and we have defined

$$d = \frac{1}{\beta_1 \pi} a \tag{31}$$

where $\beta_1\pi$ is the lowest zero of the Bessel function, $J_0(\beta_1\pi) = 0$, so that

$$d = 0.4161a \tag{32}$$

Although Eq. 30 appears arbitrary at first sight, it will be shown immediately that from it results a simple analytical expression of the full solution.

In both indicated cases the reference for potential ϕ is given by the quasi-neutral region of the substrate.

Potential distribution in the columnar semiconductor

The procedure of the solution of the differential equations 25 and 26 has been detailed in the Appendix. The results are given here. For the Laplace part of the solution we have, on the one hand, from Eqs. 28 and 29:

$$\phi^{\mathscr{L}\mathrm{I}}(r,z) = \phi_\mathrm{s} - (\phi_\mathrm{s} - \phi_\mathrm{j}) \times \sum_{m=1}^{\infty} \frac{2}{\beta_m \pi} \frac{J_0(r/\eta_m)}{J_1(\beta_m \pi)} \exp(-z/\eta_m) \tag{33}$$

Here the numbers $\beta_m\pi$ are the zeroes of the Bessel function (see Appendix), J_1 is the Bessel function of order one, and

$$\eta_m = \frac{1}{\beta_m \pi} a \tag{34}$$

Furthermore, Eq. 33 requires that $\eta_m \ll L$, which is warranted by our previous assumption that $a \ll L$. On the other hand, from Eqs. 28 and 30 there results

$$\phi^{\mathscr{L}\mathrm{II}}(r,z) = \phi_\mathrm{s} - (\phi_\mathrm{s} - \phi_\mathrm{j})J_0(r/d)\exp(-z/d) \tag{35}$$

Regarding the Poisson part of the solution, the solution of Eqs. 26 and 27 is

$$\phi^{\mathscr{P}}(r,z) = -\frac{8}{\pi^3 L_\mathrm{D}^2} \sum_{m=1}^{\infty} \frac{1}{\beta_m \pi} \frac{J_0(\beta_m \pi r/a)}{J_1(\beta_m \pi)} \times \sum_{p=0}^{\infty} \frac{1}{(2p+1)} \frac{1}{[(2p+1)/L]^2 + [\beta_m/a]^2} \times \sin[(2p+1)\pi z/L] \tag{36}$$

The final results are

$$\phi^{\mathrm{I}}(r,z) = \phi^{\mathscr{L}\mathrm{I}}(r,z) + \phi^{\mathscr{P}}(r,z) \tag{37}$$

and

$$\phi^{\mathrm{II}}(r,z) = \phi^{\mathscr{L}\mathrm{II}}(r,z) + \phi^{\mathscr{P}}(r,z) \tag{38}$$

In the 3-dimensional plots in Fig. 4 we represent ϕ^I and ϕ^II for $a = L_\mathrm{D}, L = 10a$, $\phi_\mathrm{j} = 5$ and $\phi_\mathrm{s} = 15$. Each summation in Eqs. 33 and 36 has been computed using the 20 first terms in the summatories. The reduced potential distribution is better analysed separately in two zones.

Potential near the back contact

Figure 4 shows that most of the total internal potential drop falls in the close vicinity of the back contact. Comparing Figs. 4a and b it is appreciated that no essential differences in the overall potential distribution exist between ϕ^I and ϕ^II. A crucial issue is the total penetration of the electric field in the electrode, which is of the order of $2a$ in both examples. Note in Eq. 33 that the characteristic penetration distance associated with each term is η_m, and that the largest of these numbers is $d = \eta_1$, which is the only one appearing in Eq. 35. In forthcoming computations involving the potential distribution, we combine the most advantageous features of both ϕ^I and ϕ^II. We assume an electric field essentially homogeneous in the radial direction, as in Fig. 4a; this conveniently turns the problem into a one-dimensional situation. Hence it is enough to perform the computations at the cylinder axis, and for that purpose we use the expression of ϕ^II, which is simpler.

The potential along the axis is shown in Fig. 5. The representation confirms that the large rise of potential near the back contact, which originates from the Laplace part of the solution, takes place in a distance ca. $2a$. It is apparent from Eq. 35 that the characteristic distance d of penetration is independent of the internal potential drop in the electrode $\phi_\mathrm{s} - \phi_\mathrm{j}$.

Potential far from the flat boundaries

At points far from the flat boundaries ($2a < z < L - 2a$) there is no potential gradient along the axial direction. There is nonetheless a small curvature along the radial direction, stemming from the Poisson part of the solu-

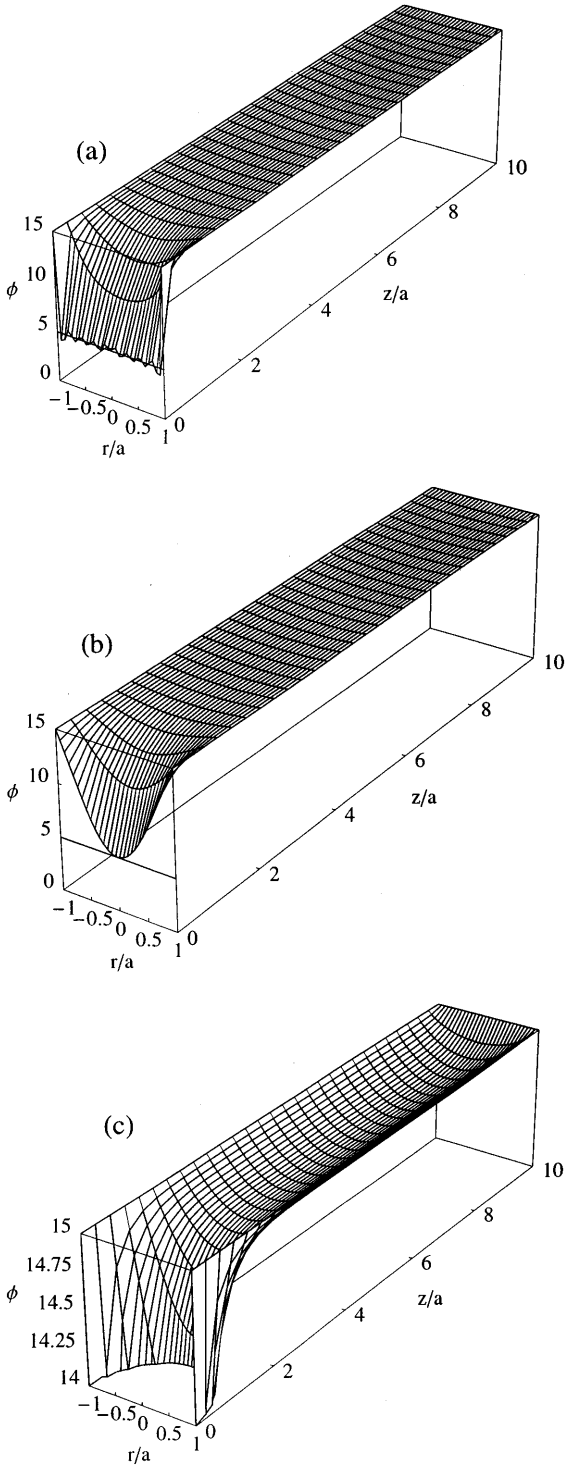

Fig. 4a–c The reduced potential ϕ in a longitudinal section of a fully depleted cylindrical semiconductor particle for $a = L_D$, $L = 10a$, $\phi_j = 5$ and $\phi_s = 15$. All distances are scaled to the radius of the cylinder a. **a** Representation of ϕ^I. Note that $\phi \approx 5$ at the surface in contact with the substrate $z = 0$ (the exact result is $\phi = 5$), whereas $\phi = \phi_s$ at the rest of surfaces. **b** Representation of ϕ^{II}. **c** Enlarged view of **a** showing the interval of potential $\phi_j + 0.9(\phi_s - \phi_j) \leq \phi \leq \phi_s$

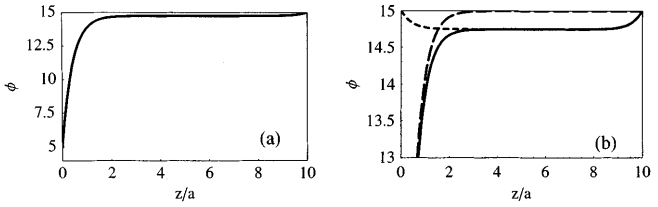

Fig. 5a, b The reduced potential ϕ^{II} along the axis $r = 0$ of a fully depleted cylindrical semiconductor particle, for $a = L_D$, $L = 10a$, $\phi_j = 5$ and $\phi_s = 15$. **a** View of the full range of potential. **b** Enlarged view showing the potential interval $\phi_j + 0.9(\phi_s - \phi_j) \leq \phi \leq \phi_s$. *Continuous line*: full solution. *Short dashes*: Poisson part of the solution, $\phi^{\mathscr{P}}$. *Long dashes*: Laplace part of the solution, $\phi^{\mathscr{L}II}$

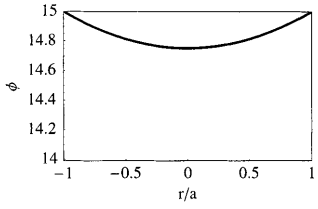

Fig. 6 The reduced potential ϕ along the radial direction (z = constant, far from the planar boundaries) of a fully depleted cylindrical semiconductor particle; same example as shown in Fig. 5

tion. This is seen in Fig. 4c. The radial distribution of potential in the region $2a < z < L - 2a$ is shown in Fig. 6. Owing to symmetry under translation in the z direction, in this zone of the cylinder we can derive the potential distribution with a simple approach, similar to that of A-B seen above. We solve, from Eq. 26:

$$\frac{1}{r}\frac{\partial}{\partial r}\left(r\frac{\partial \phi}{\partial r}\right) = \frac{1}{L_D^2} \tag{39}$$

with boundary conditions $\partial\phi/\partial r = 0$ at $r = r_w$ and $\phi(a) = \phi_s$. The result is

$$\phi(r) = \phi_s - \frac{1}{L_D^2}\left(\frac{1}{4}(a^2 - r^2) - \frac{r_w^2}{2}\ln\frac{r}{a}\right) \tag{40}$$

and for the case of full depletion $r_w = 0$ we obtain

$$\phi(r) = \phi_s - \frac{1}{4L_D^2}(a^2 - r^2) \tag{41}$$

This is the solution plotted in Fig. 6; actually using in Eq. 36 only the first three terms in β_m we obtain an excellent approximation to Eq. 41. Hence as regards points located at $z \gg a$, no significant difference exists between the sphere and the column models, in accordance with the reasoning presented earlier. The potential drop between the centre and the surface is now

$$\Delta\phi_M = \frac{1}{4}\left(\frac{a}{L_D}\right)^2 \tag{42}$$

a result similar to that in Eq. 21.

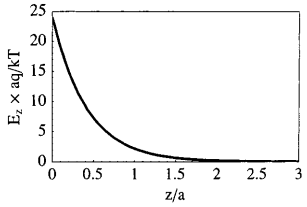

Fig. 7 The reduced electric field F along the axis $r = 0$ of a fully depleted cylindrical semiconductor particle

The electric field

In general, the expression of this magnitude is obtained taking the derivative of the electric potential

$$\boldsymbol{E} = -\nabla V \tag{43}$$

Next we calculate the value of the field along the axis $r = 0$. We will use the reduced field

$$F = \frac{aq}{kT} E_z = a \frac{\partial \phi}{\partial z} \tag{44}$$

When $a < L_D$ ($\Delta\phi_M \ll \phi_s - \phi_j$) the contribution of the Poisson part of the solution can be neglected. Hence from Eq. 35 the potential is

$$\phi(z) = \phi_s - (\phi_s - \phi_j)\exp(-z/d) \tag{45}$$

and from Eq. 44 we get

$$F(z) = (\phi_s - \phi_j)\frac{a}{d}\exp(-z/d) \tag{46}$$

Equation 46 is represented in Fig. 7. We check again that the distance over which the electric field extends is about $4d \approx 2a$. Note from Eq. 46 that the electric field at the interface is proportional to the internal potential difference. This reflects the constancy of the characteristic penetration distance d. By contrast, the electric field at the outer edge of the classical depletion zone varies as the square root of the internal potential; see Eqs. 48 and 49 below.

The heterojunction at the back contact

It has been noted that the potential drop ϕ_s need not reside entirely in the assembly of TiO_2 particles. Rather, a depletion region may be formed in the transparent conducting oxide, an effect that has been well documented in the related case of the ITO/polycrystalline TiO_2 system [22]. It is of central importance to the problem presently under study to evaluate the potential ϕ_j at the junction between the electrode and the transparent conducting oxide, for as we have just seen, the larger the fraction of the potential in the porous semiconductor, the more the strength of the electric field in it. The transparent conducting oxide is frequently a degenerate n-type semiconductor, in which case Boltzmann statistics do not apply in the *quasi-neutral* region, but nonetheless the Schottky model as given by Eqs. 14–16 correctly describes the potential in the *depletion* zone provided one notes that $\zeta_c = 0$ and $n_b \approx N_c$; these values can be shown to give a reasonable approximation in the light of Fermi-Dirac statistics [23]. In fact the capacitance of bare transparent semiconductor electrodes such as ITO has been measured [24], and good Mott-Schottky curves resulted from the analysis.

Distribution of potential at both sides of the heterojunction

It follows from the preceding remarks that the situation, illustrated in Fig. 8, consists of a totally depleted heterojunction [17, 22]. In the substrate side we have a depletion zone which extends a distance w. The potential is given by Eq. 14, which adapted to Fig. 8 turns into

$$\phi(z) = 0 \qquad (z \le -w) \tag{47}$$

$$= \frac{1}{2L_{D1}^2}(z + w)^2 \quad (-w \le z \le 0)$$

with $\phi(0) = \phi_j$ and hence

$$w = (2\phi_j)^{1/2} L_{D1} \tag{48}$$

From Eq. 47 we obtain the reduced field

$$F(z) = 0 \qquad (z \le -w) \tag{49}$$

$$= \frac{1}{L_{D1}^2}(z + w) \quad (-w \le z \le 0)$$

In the electrode side the potential is given by Eq. 45. The two solutions have to be matched by the condition

$$\epsilon_1 E_z(0^-) = \epsilon_2 E_z(0^+) \tag{50}$$

that is

$$\epsilon_1 \left.\frac{\partial \phi}{\partial z}\right|_{0^-} = \epsilon_2 \left.\frac{\partial \phi}{\partial z}\right|_{0^+} \tag{51}$$

It is implicitly assumed in Eq. 51 that the interface is devoid of surface states. A recent treatment that includes

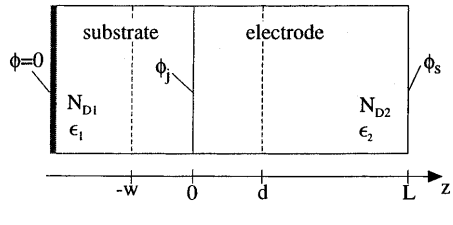

Fig. 8 Representation of the columnar electrode of length L and conducting substrate, forming a totally depleted heterojunction. The junction is at $z = 0$. The width of the depletion zone in the substrate is w, and d is the characteristic distance of penetration of the electric field into the column. Doping levels and dielectric constants are: for the substrate, N_{D1} and ϵ_1; for the electrode, N_{D2} and ϵ_2

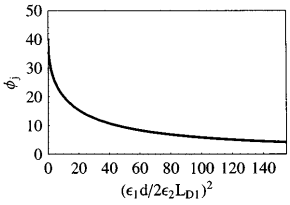

Fig. 9 The potential at the interface substrate/electrode, for a total potential drop $\phi_s = 40$, as a function of characteristic parameters indicated in Fig. 7 and in the text

this effect is given in [25]. From Eqs. 45, 47, 48 and 51 we obtain

$$\sqrt{2}\frac{\epsilon_1 d}{\epsilon_2 L_{D1}}\phi_j^{1/2} = \phi_s - \phi_j \tag{52}$$

Introducing the parameter

$$b = \left(\frac{\epsilon_1 d}{\epsilon_2 L_{D1}}\right)^2 \tag{53}$$

we can write the solution of Eq. 52 as

$$\phi_j = \phi_s - b\left[\left(1 + \frac{2\phi_s}{b}\right)^{1/2} - 1\right] \tag{54}$$

This is the final result that dictates how the two media share the total drop ϕ_s. We find two limiting cases: for $b \approx 0$ we obtain $\phi_j \approx \phi_s$, whereas for $b > 10\phi_s$ we have $\phi_j \approx \phi_s^2/2b$. Equation 54 is plotted in Fig. 9 for a total drop $\phi_s = 40$. Giving values to the relevant parameters, we can now plot the potential, the electric field and the energy of the conduction band edge. This is done in Fig. 10, where the parameter values have been chosen so as to facilitate visualization.

More realistic figures are: $N_{D1} = 10^{20}\,\mathrm{cm}^{-3}$ and $\epsilon_1 = 8\epsilon_0$ for the substrate, where ϵ_0 is the permittivity of vacuum, giving $L_{D1} = 0.3$ nm, and for the TiO_2 electrode $N_{D2} = 10^{17}\,\mathrm{cm}^{-3}$, $\epsilon_2 = 130\epsilon_0$ yielding $L_{D2} = 43$ nm and $\zeta_c \approx 10$. Considering that the radius of the particles is $a = 10$ nm, we have $d = 4$ nm and $b = 2.2$. For a total voltage drop $V_s = -1$ V, corresponding to $\phi_s = 40$, we obtain from Eq. 54 $\phi_j = 34$. Hence 15% of the total voltage difference is in the electrode in this example, and the width of the depletion zone in the substrate is $w \approx 3$ nm. Finally, an estimation of the electric field strength in the electrode can be obtained from Eqs. 44 and 46:

$$E_z(0^+) = -\frac{kT}{qd}(\phi_s - \phi_j) \tag{55}$$

giving $E_z(0^+) = 4 \times 10^5\,\mathrm{V\,cm}^{-1}$.

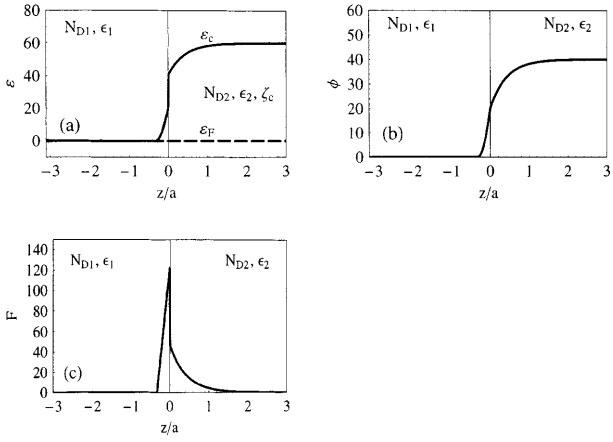

Fig. 10 Representation of **a** the energy bands, **b** the reduced potential, and **c** the electric field, in a columnar electrode in contact with a substrate. Distances are scaled to radius of columnar electrode $a = L_{D2}$, and the total potential drop is $\phi_s = 40$. The material parameters are: for the substrate, $N_{D1} = 10^{19}\,\mathrm{cm}^{-3}$, $\epsilon_1 = 8\epsilon_0$ and $\zeta_c = 0$; for the electrode, $N_{D2} = 10^{17}\,\mathrm{cm}^{-3}$, $\epsilon_2 = 30\epsilon_0$, and $\zeta_c = 20$

Discussion and conclusions

Peculiar properties appear in the distribution of the electric potential in nanocrystalline particulate semiconductor electrodes, with no counterpart in a planar electrode. A strikingly clear demonstration in this respect was provided by studies on crystalline GaP porous networks by Vanmaekelbergh and co-workers [21, 26]. At low band bending, the depletion layer is so thin that it follows the surface of the pores, but once the entire porous layer is depleted (at larger positive applied potential) it no longer contributes to the differential capacitance. The experimental signature of this effect is a change of slope in the Mott-Schottky plot.

To gain insight into this type of phenomenon, we have worked out a model for the three-dimensional distribution of electric potential in a chain of nanoparticles connected to an electrode at one end and surrounded with a liquid material. As a suitable approach to the complex geometry we assume axial (cylindrical) symmetry. This assumption, which is in line with that adopted in previous studies on related systems [16, 21], turns the problem into a reasonable two-dimensional calculation which can be effected analytically. Nonetheless, a direct confrontation of the model with experiment appears feasible, since the fabrication of tubular semiconductor particles in the ultrasmall scale is already being envisioned by some workers.

In depletion conditions, and in equilibrium (no charge transport), the donor density fixes at every point the curvature of the electric potential. Ions in the surrounding medium play no role in this respect: this ensues from the local nature of Poisson's equation. However, ion distribution in the liquid is able to exert an influence over the inner electric field through the boundary conditions. Here we have set the simplest boundary condition (an equipotential at the distributed porous surface), and the effect of more complex conditions is an issue that remains to be investigated. Keeping this provision in mind, several major conclusions can be extracted from the model that has been presented.

The first is that a significant part of the total potential drop can be accommodated in the semiconducting array of particles. This result follows from detailed consideration of basic principles, and it is in contrast to a widely held notion that was concluded on the basis of a single sphere model. The important consequence ensues that we need not invoke an unreasonably large potential drop at the Helmholtz layer.

A second conclusion is that the potential distribution is exactly the opposite with respect to the planar electrode case, as regards both the electric field location and the band curvature, cf. Figs.1 and 5. In a semiconductor column with a radius smaller than the extrinsic Debye length, the field is agglomerated at the back contact. The role of this field is crucial in that the corresponding voltage drop shifts downwards the Fermi level with respect to the conduction band in the rest of the electrode, so that full depletion and essentially flat bands are attained there. Furthermore, and importantly, this general picture about the electric field distribution is entirely consistent with the results of detailed experiments that investigated the issue, viz. electroreflectance measurements by Goossens and co-workers [9], and the electrochemical impedance spectroscopy and dye-desorption experiments by Gregg and co-workers [8]. Both groups have concluded that in a TiO_2 nanocrystalline porous electrode in dark conditions an electric field is observed near the back contact when a positive potential is applied.

The third main consequence of the model shows again an important difference with the planar electrode case. In the latter the region along which the internal potential drop is distributed (space-charge or depletion region) grows steadily as the amount of internal potential drop is increased. This lies at the root of the widely used capacitance-voltage technique, which provides important information on band structure via the interpretation of Mott-Schottky plots. In its turn, in the depleted semiconductor column the electric field augments in strength as the internal potential difference increases, but the region in which a non-negligible field exists maintains an unchanging size of the order of the radius of the particle.

It is interesting to observe that these differences between the planar and the nanoporous electrode cases stem from the fact that entire depletion occurs in a system only if the quantity $(2\phi_s)^{1/2}L_D$ is of the order of the "minimal size" available. In the nanoporous electrode this minimal size is the radius of the particle, whereas in an planar homogeneous electrode it is the thickness of the electrode. This implies that the internal potential drop necessary to cause full depletion is substantially larger in the latter case than in the former.

From these considerations, some indications follow regarding the more general problem of transport theories under illumination. As we commented at the beginning, in the Gärtner-Butler model the background Schottky barrier-type field in the dark is unaffected by photogenerated carriers. This has been assumed in the original calculations by Butler [1] and also in most of the later more refined treatments [27]. Contrarily, the scenario depicted in terms of the column model appears to be unstable under intense illumination. Photogenerated carriers can modify substantially the distribution of potential in the dark. Therefore if under illumination there exist electric fields that drive the charge carriers concurrently with concentration gradients, those electric fields may be sustained, at least in part, by the distribution of the carriers that maintain the photocurrent.

Appendix

We wish to determine the electrostatic potential ϕ in a homogeneously charged cylindrical particle of radius a and length L. We have to solve Eqs. 23–28, with an additional boundary condition that specifies the potential at the circle $z = 0$. We take first the Laplace part of the solution. We fix the value of ϕ at the *central point* of the base circle $z = 0$, by means of

$$\phi^{\mathscr{L}}(0,0) = \phi_j \tag{A1}$$

and we write the solution as

$$\phi^{\mathscr{L}}(r,z) = \phi_s - (\phi_s - \phi_j)\varphi(r)\psi(z) \tag{A2}$$

Applying the method of separation of variables, Eq. 25 splits into two equations:

$$\frac{\partial^2\psi}{\partial z^2} - \frac{1}{\eta^2}\psi = 0 \tag{A3}$$

$$\frac{1}{r}\frac{\partial}{\partial r}\left(r\frac{\partial\varphi}{\partial r}\right) + \frac{1}{\eta^2}\varphi = 0 \tag{A4}$$

where η^2 is a positive constant to be determined. The boundary conditions of Eqs. 28 and A1 impose that

$$\psi(0) = 1; \quad \psi(L) = 0 \tag{A5}$$

and also

$$\varphi(0) = 1; \quad \varphi(a) = 0 \tag{A6}$$

The solution of Eqs. A3 and A5 is

$$\psi(z) = \exp(-z/\eta) \tag{A7}$$

provided $L \gg \eta$, which is justified if $L \gg a$. The solution of Eqs. A4 and A6 is

$$\varphi(r) = J_0(r/\eta) \tag{A8}$$

where J_0 is the Bessel function of zero order. Equation A6 requires also that

$$J_0(a/\eta) = 0 \tag{A9}$$

and thus $\eta_m = a/\beta_m\pi$, where the numbers $\beta_m\pi$ are the zeroes of the Bessel function, $J_0(\beta_m\pi) = 0$, marked so that $\beta_m < \beta_{m+1}$, with the values $\beta_1 = 0.7655$, $\beta_2 = 1.7546$, $\beta_3 = 2.7546$, and $\beta_m \cong m - 1/4$ for $m \gg 0$ [28]. We can write the solution of Eq. 25 as a linear combination:

$$\phi^{\mathscr{L}}(r,z) = \phi_s - (\phi_s - \phi_j) \times \sum_{m=1}^{\infty} A_m J_0(r/\eta_m)\exp(-z/\eta_m) \tag{A10}$$

which satisfies the required boundary conditions of Eqs. 28 and A6 if

$$\sum_{m=1}^{\infty} A_m = 1 \tag{A11}$$

is fulfilled. The undetermined coefficients A_m reflect the fact that, so far, the values of Eq. A10 in the contact circle ($z = 0$) have been specified only at the centre and at the edge, that is

$$\phi^{\mathscr{D}}(r,0) = \phi_s - (\phi_s - \phi_j) f(r) \tag{A12}$$

where

$$f(r) = \sum_{m=1}^{\infty} A_m J_0(r/\eta_m) \tag{A13}$$

with values at the extremes

$$f(0) = \sum_{m=1}^{\infty} A_m = 1; \quad f(a) = 0 \tag{A14}$$

Once f is given the coefficients A_m can be determined using Eq. A13 and the orthogonality properties of the Bessel functions. A first choice consists in setting the circle at the contact at a potential ϕ_j:

$$\begin{aligned} f^{\mathrm{I}}(r) &= 1 \quad r < a \\ &= 0 \quad r = a \end{aligned} \tag{A15}$$

The full solution is given in Eq. 33. As a second choice we take only the first term in the summatory of Eq. A13:

$$f^{\mathrm{II}}(r) = J_0(r/d) \tag{A16}$$

where d is defined in Eq. 31. The corresponding solution is given in Eq. 35.

To find out the Poisson part of the solution, the pertinent Green function, which is given in [29], is integrated over the whole cylinder volume. The result is given in Eq. 36.

Acknowledgements It is a pleasure to express our gratitude to Professor P. Salvador for useful discussions and advice. We are also thankful to Professor F. García Moliner for discussing this work with us. The Fundació Caixa-Castelló is gratefully acknowledged for largely supporting these studies.

References

1. Butler MA (1977) J Appl Phys 48: 1914
2. Gärtner WW (1959) Phys Rev 116: 84
3. O'Regan B, Moser J, Anderson M, Grätzel M (1990) J Phys Chem 94: 8720
4. Albery WB, Bartlett PN (1984) J Electrochem Soc 131: 315
5. O'Regan B, Moser J, Anderson M, Grätzel M (1990) J Phys Chem 94: 8720
6. Hagfeldt A, Grätzel M (1995) Chem Rev 95: 49
7. Södergren S, Hagfelt A, Olsson J, Lindquist S-E (1994) J Phys Chem 98: 5552
8. Zaban A, Meier A, Gregg BA (1997) J Phys Chem B 101: 7985
9. Boschloo GK, Goossens A, Schonman J (1997) J Electroanal Chem 428: 25
10. Dloczik L, Ileperume O, Lauerman I, Peter LM, Ponomarev EA, Remond G, Shaw NJ, Uhlendorf I (1997) J Phys Chem, 101: 10281
11. Enright B, Fitmaurice D (1996) J Phys Chem 100: 1027
12. Hodes G, Howell IDJ, Peter LM (1992) J Electrochem Soc 139: 3136
13. Hagfelt A, Björkstén U, Lindquist S-E (1992) Sol Energy Mat Sol Cells 27: 293
14. Lindquist S-E, Finnström B, Tegnér L (1983) J Electrochem Soc 130: 351
15. Cao F, Oskam G, Meyer G, Searson PC (1996) J Phys Chem 100: 17021
16. Cao F, Oskam G, Searson PC, Stipkala JM, Heimer TA, Farzad F, Meyer GJ (1995) J Phys Chem 99: 11974
17. Levy B, Liu W, Gilbert SE (1997) J Phys Chem 101: 1810
18. Mönch W (1995) Semiconductor surfaces and interfaces, 2nd edn. Springer, Berlin Heidelberg New York
19. Nozik A, Memming R (1996) J Phys Chem 100: 13061
20. Grätzel M (1989) Heterogeneous photochemical electron transfer. CRC Press, Boca Raton
21. Erne BH, Vanmaekelbergh D, Kelly JJ (1996) J Electrochem Soc 143: 305
22. van de Krol R, Goosens A, Schoonman J (1997) J Electrochem Soc 144: 1723
23. Seeger K (1991) Semiconductor physics, 5th edn. Springer, Berlin Heidelberg New York
24. Meeraker JEAM, Meulenkamp EA, Scholten M (1993) J Appl Phys 74: 3282
25. Goren B, Nemirovsky Y (1995) J Appl Phys 77: 244
26. Vanmaekelbergh D, Iranzo Marín F, van de Lagemaat J (1996) Ber Bunsenges Phys Chem 100: 616
27. Salvador P (1984) J Appl Phys 55: 2977
28. Abramowitz M, Stegun IA (1965) Handbook of mathematical functions. Dover, New York
29. Morse PM, Feshbach H (1953) Methods of theoretical physics, vol 2. McGraw-Hill, New York